RSC Applied Interfaces

ROYAL SOCIETY OF CHEMISTRY

PAPER

View Article Online
View Journal | View Issue

Cite this: *RSC Appl. Interfaces*, 2025, **2**, 1473

Paint adhesion on titanium and zirconium oxide conversion coated galvanised steel

Laura-Marleen Baumgartner,*[ab] Andreas Erbe [c] and Michael Rohwerder[b]

The effect of cleaning and rinsing on the formation of titanium and zirconium oxide based conversion coatings was investigated. The conversion coatings were applied by coil coating on hot-dip galvanised steel (Z), electrolytic galvanised steel (ZE) and the novel zinc–magnesium–aluminium alloy coated steel (ZM). Consequences on paint adhesion were also studied. Two different conversion coating solutions were used which differ in pH as well as in their chemical composition. Both solutions are titanium oxide based where as one contains a zirconium compound in addition. Glow discharge optical emission spectroscopy (GDOES) confirmed that the addition of rinsing steps during the coating process removes significant amounts of coating components from all surfaces. The coating weight varies depending on the different cleaning and substrate and is highest on ZM when using the titanium based conversion coating. The adhesion test results of the full-coat system show a good correlation between the conversion coating wetting behaviour, the effect of inclusion of a rinsing step into the coating process and paint adhesion as tested qualitatively by a water-storage test for a duration of 1008 h. Independent of cleaning and pretreatment, the traditional ZE showed excellent performance. Paint adhesion on ZM was best after acidic cleaning, pretreatment without zirconium oxide, and rinsing. For Z, the zirconium-oxide free coating also showed strongest adhesion, independent of cleaning. Industrial substrates were compared with model substrates consisting of vapour deposited zinc, magnesium or aluminium. Clear differences in the arising conversion layer build-up structures were observed by scanning electron microscopy (SEM); no typical conversion layer structure was found on aluminium. Consequently, the aluminium component of the mixed surface oxide is hypothesised to slow down conversion coating formation during coil coating.

Received 21st January 2025,
Accepted 30th July 2025

DOI: 10.1039/d5lf00011d

rsc.li/RSCApplInter

1 Introduction

The passivation of steel and galvanised steel by conversion coatings (CCs) is an important process to protect the metallic substrate from corrosion.[1–3] In different areas of application, an additional layer is required to protect these materials against corrosion in a multi-layer coating system, and to prepare the surface for further coatings.[1,4–6] A CC is usually applied after an alkaline cleaning step on the surface. The conversion process transforms the surface in a way that a chemical bond can be formed with subsequent layers. Modern CCs are often based on titanium or zirconium oxides which are replacing phosphates. On the one hand, there are phosphating solutions that consist primarily of alkali metal phosphates and the conversion layer on the zinc surface is created through the direct involvement of the base metal in the process. On the other hand, there are solutions based on metal phosphates, mainly iron, zinc and manganese, with the layer being formed by the metal cations present in the solution. The latter is the dominant technology in the field of phosphating, but there are ecological concerns on the extensive use of phosphates. The new generation of surface treatments based on titanium or zirconium increases the corrosion protection, frequently by improving paint adhesion.[5,7–20]

The interactions at the interface between a steel surface during the pretreatment play a crucial role in the formation of the conversion layer and the resulting corrosion resistance.[21] The conversion process itself occurs on a minute time scale and the resulting layer is, with a few tens to hundred nanometres, thin. A typical pretreatment bath contains hexafluorozirconic acid or hexafluorotitanic acid and additional components to adjust the pH.[6,18,19] Inorganic additives may affect deposition rate and morphology.[20,22] Zinc and its alloys are easily attacked by fluorides, dissolve during the layer growth, and their products may get built into the conversion layer.[18,20,23–25] Organic additives are added to

[a] *thyssenkrupp Steel Europe AG, Eberhardstr. 12, 44145 Dortmund, Germany*
[b] *Department of Interface Chemistry and Surface Engineering, Max Planck Institute for Sustainable Materials, Max-Planck-Str. 1, 40237 Düsseldorf, Germany. E-mail: adhesion-on-galv@the-passivists.org*
[c] *Department of Materials Science and Engineering, NTNU, Norwegian University of Science and Technology, 7491 Trondheim, Norway*

the conversion bath to improve the adhesion to subsequent layers and to increase homogeneity of the coating.[19,26–29] The combined effect of organic and inorganic additives leads to a complex internal structure of the CCs.[25,30–34]

One way to apply a CC in a laboratory is to immerse the substrate into the CC bath, whereby in a first step the native oxide layer of the metal surface needs to be dissolved.[6,18–20] This leads to a local increase in pH which can lead to the precipitation of metal (hydr)oxides, *e.g.* titanium- or zirconium oxides.[18,35,36] The pH has a huge impact on the layer formation and was described in several studies to be in the range 1.5–6.[9,11,13,14,36]

Depending on the application, different substrates are used. An electrolytic galvanised steel (ZE) surface consists of zinc crystals and has a high surface area.[1,3] The microstructure of a hot-dip galvanised steel (Z) is coarser and primarily single-phased consisting of zinc crystals. There is the possibility of additional aluminium-containing phases as the galvanising bath contains a small fraction of aluminium.[1,3] Aluminium addition in Z leads to aluminium oxide containing surfaces.[34,37] New materials represented by zinc alloys containing both aluminium and magnesium (ZM) find more and more application because of their excellent corrosion resistance. Some modern variants also include silicon.[38] ZM coatings have a rather complex, heterogeneous surface,[34,39] and they are less investigated compared to the more traditional ZE and Z. Alloys used for ZM coatings have zinc-rich primary crystals with intervening eutectic areas.[39] A differentiation can be made between the primary zinc phase, a binary eutectic of zinc and $MgZn_2$ and a ternary eutectic including aluminium.[39,40] The arising oxide layer consists for the most part of aluminium and magnesium which is the main difference to galvanised steel.[37,39,40] Both materials, Z and ZM undergo the skin-pass rolling during the production process. It is the final forming step and has a significant influence on the materials mechanical properties as well as surface topography.[41]

Despite the fact that all three metallic coatings are zinc-based, the surface oxides of the three show significant differences because of alloying of aluminium (Z,ZM) and magnesium (ZM).[39] The most oxygen affine element in ZM alloys is magnesium, followed by aluminium. Therefore, one finds a higher concentration of magnesium oxide than aluminium oxide. There is indication for the formation of an alternative compound inside the oxidic layer which is $MgAl_2O_4$ spinel. The skin passing procedure leads to a breakage of the oxide layer into fragments and native oxide layers will be formed immediately.[40] In comparison the formation of Al_2O_3 oxide layers on the surface of Z has been observed.[40] As opposed to Al_2O_3, MgO is quite stable at alkaline pH, which may pose challenges for subsequent coating adhesion. A key hypothesis in this work bases on observations for other systems, where the enrichment of magnesium during alkaline treatment poses adhesion challenges. The investigation on whether acid cleaning is more appropriate for magnesium-containing metallic coatings is a consequent main driver for this study.

The main focus of this work is to compare qualitatively the pretreatment process of these different metallic coatings on steel, with main focus on the novel ZM. A detailed study of the microstructure of very similar coatings, and the effect different cleaning procedures have on the surface composition, is already available.[39] For a fundamental understanding of the formation mechanisms and the effect on performance, model surfaces of the pure elements included in the alloys, zinc, aluminium and magnesium, were investigated. Resulting conversion coated surfaces were imaged by scanning electron microscopy (SEM). General hypotheses about reactions taking place during the conversion process of the used titanium or zirconium oxide based CCs exist,[6] however, the contact time during production in a coating line is only a few seconds, thus much shorter than exposure times typically studied. Typical speeds are between 10 to 200 m min^{-1};[4] on this time scale, the wetting kinetics may play an important role. Continuous processes also include the challenge that it is not possible to extract samples on all desired intermediate stages, making comparisons challenging. To investigate the importance of conversion time, a further rinsing step was added into the coating process. Coating weights were then detected with glow discharge optical emission spectroscopy (GDOES). Coating adhesion at different stages was compared qualitatively. Detailed electrochemical studies and more detailed corrosion product characterisation—despite valuable—were not part of this work.

2 Experimental

2.1 Substrates

Steel substrates with thicknesses around 0.7 mm were provided from thyssenkrupp Steel Europe AG hot-dip coating lines. Galvanised steel (Z; 1–2 wt% Al) has a specific coating mass of 42 g m^{-2} and zinc–magnesium–aluminium alloys (ZM; 1–2 wt% Mg and 1–2 wt% Al) have a specific coating mass of 37 g m^{-2}. In addition, electrolytic galvanised steel (ZE) with a coating thickness 8 μm was used. In the original state, samples contained a corrosion protection oil which is removed in a cleaning step first. The oiling is part of the semi-continuous production process and made it hard to include meaningful surface characterisation of samples without cleaning. For ZM as the substrate with the largest novelty only, few samples before oiling have been extracted.

2.2 Cleaning

Substrates were either cleaned by an alkaline cleaning step at 60 °C or in an acidic cleaning step at room temperature. For alkaline cleaning a spray cleaning was used whereas an immersion cleaning was used with the acidic cleaning solution. In both cases the samples have been rinsed with tap water and deionised water afterwards. The pH of the

alkaline solution was between 12.4–13.2 and around 1.0 for the acidic cleaning solution.

2.3 Pretreatment

This work focuses on a comparison between a standard pretreatment (PT 2) solution which is commonly used for decades in the coil-coating industry and a relatively new one for universal applications (PT 1). Both are hexafluorotitanic acid based with an acidic pH and both contain phosphates. PT 2 contains in addition a hexafluorozirconic acid as well as hydrofluoric acid. PT 1 has added polyacrylic acid instead and has a pH at around 1.7 whereas PT 2 has a higher pH at around 3. Both PT 1 and PT 2 contain different fluoride ion releasing components which affect the conversion process and the metal dissolution. Metal dissolution is in addition facilitated by the fluoride-assisted breakdown of the oxide layers.

Pretreatment was performed with a laboratory roll coater to achieve thin films which have been dried in a continuous furnace at 70–80 °C peak metal temperature afterwards. The coating's target weight of phosphorous is between 5–10 mg m^{-2} for PT 1 and of titanium between 6–10 mg m^{-2} for PT 2. Marker elements and their respective target weights are defined by the coating manufacturers. Usually there is no rinsing step in the standard coil-coating process after application of these pretreatment solutions. To check coating adhesion at different steps in the process, a rinsing step was inserted into the process. A distinction is made between the rinsing directly after the laboratory roll coater and the rinsing after drying in a continuous furnace (see Table 1). After initial investigations of the state of the art industrial processes on ZM, adhesion was not always satisfactory, which is why the rinsing step was introduced. Rinsing may remove loosely bound species from the CC which could potentially improve adhesion, as without rinsing, all components remain in the system. After rinsing all substrates have been dried. All samples were prepared in duplicate. An overview over the sequence of all preparation steps is given in Fig. 1.

2.4 Model surfaces

Silicon wafers were used and coated with the respective elements zinc, aluminium or magnesium using physical vapor deposition. In a second step these samples have been coated with PT 1 using a laboratory spin coater and dried in a fume hood for 24 h. Pictures of the surfaces were taken with a standard single-lens reflex camera. Illumination conditions and viewing conditions were kept the same. Pictures were always taken in the same room.

Table 1 Abbreviations of rinsing steps

Rinsing step	Abbreviation
No rinse	n. r.
After roll coater	a. c.
After drying	a. d.

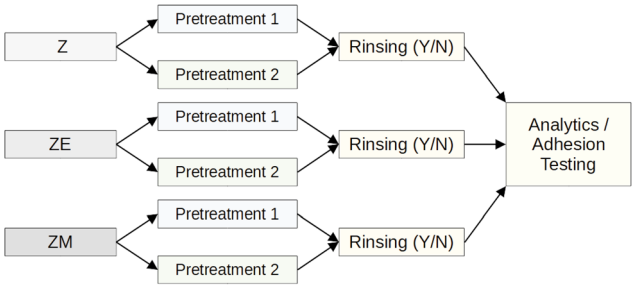

Fig. 1 Flow chart showing the overall study design in this work.

2.5 Methods

For evaluation of the surface roughness of the different substrates after the usage of various cleaning solutions atomic force microscopy (AFM) was conducted using a Veeco Digital Instruments NanoScope with an Olympus micro cantilever in tapping mode. The determined surface roughness was compared using the Sdr-value as defined in ISO 25178 as

$$\mathrm{Sdr} = \frac{1}{A}\left[\iint_A \left(\sqrt{1+\left(\frac{\partial z(x,y)}{\partial x}\right)^2+\left(\frac{\partial z(x,y)}{\partial y}\right)^2}-1\right)\mathrm{d}x\mathrm{d}y\right], \quad (1)$$

where height z as function of spatial coordinates x and y over the projected flat area A is used. Sdr = 0 indicates a completely flat surface without any texture. Any texture leads to an increase in the respective value. Sdr as developed interfacial area ratio is judged as particularly relevant for coating application as it quantifies the area available for coating-surface interaction relative to the projected area.

The coating weight was first determined from X-ray fluorescence measurements which were taken directly after drying. Secondly the exact amount of elements on the surfaces was determined with GDOES. Depth profiles were obtained using a Spectruma Analytik GDA 750 analyzer to determine the elemental composition up to 500 nm depth from the surface. The device-specific calibration for the elements titanium and phosphorus was used for evaluation. For imaging the CC as result of pretreatment, an SEM Zeiss Leo 1550VP was used. All samples were measured at low voltages (1 keV) and images were taken at different magnifications between 500× and 20 000×.

Qualitative adhesion tests assessing coating/metal stability were performed through a deionised water storage test for 1008 h (six weeks) at 50 °C. For the implementation of the tests, a full coat system consisting of a primer and a topcoat was needed. These two additional layers were applied with a laboratory roll coater on top of the CC. In this test, cross-cuts (1 mm) down to the galvanisation layer were prepared for coated samples. Samples were then covered with a thin foil to create a more aggressive environment around these cuts. After defined time intervals, the samples were taken out of the water, and the paint adhesion was tested with an

adhesive strip and then visually evaluated. Preparation followed approximately ISO 2409.

3 Results

3.1 Effect of cleaning on surface pretreatment

The surface morphology was investigated before a CC was applied. To that end, the surface roughness was determined with AFM after different cleaning steps. For comparison of samples, the Sdr was used which represents the developed interface ratio and corresponds to the percentage of the additional area of the domain that is because of its texture (Table 2). Significant differences are observed between the different Sdr after the different cleaning methods. It must be stressed that cleaning was required to perform these measurements so that comparisons to uncleaned surfaces cannot be performed; the different surfaces may, however, have different Sdr before cleaning. The developed surface area of ZE is highest after cleaning at pH 10. For ZM, acidic cleaning yields the most developed surface in all areas of the surface. A ZM before applying corrosion protection oil showed Sdr = 0.5%, similar to samples after alkaline cleaning. For Z, characteristic differences are observed in different areas of the surface. The deeper areas of the surface show the most developed surface after acidic cleaning. Plateau areas on the Z surface appear more or less flat, but have a slight roughness after acidic cleaning.

In addition, differences in the layer formation of both pretreatment solutions on the different substrates were observed (Fig. 2–4). Fig. 2 shows the SEM images taken of the ZE-substrate coated with PT 1 or PT 2 after alkaline cleaning and after acidic cleaning. The conversion layer formed with PT 1 is heterogeneous. A porous network is formed on the zinc crystals with different density all over the surface. Some areas on the ZE-substrate are not coated with the conversion layer at all. An acidic cleaning leads to formation of an optically denser network in the CC and in addition to more heterogeneity. PT 2 shows different structures on the ZE-substrate and leads to a homogeneous surface coverage. A thin film is building up on the zinc crystals in which particles are forming whereby more particles and more pores (encircled in Fig. 2) are observed after the acidic cleaning.

Table 2 Determined Sdr values, in %. For Z and ZM, two parts of the surface with characteristic differences were separately analysed. For Z, Fig. 3 shows the different areas, since PT 1 predominantly forms on lower lying areas ("deepening") but not on the higher areas ("plateau"). For ZM, the Sdr differs between the pure zinc phase ("Zn crystal") and the eutectic phase ("eutectic")

Substrates		Cleaning pH		
Measured area		10	12	1
ZE		28.3	19.1	17.8
Z	Plateau	0.7	0.1	0.1
	Deepening	3.3	3.0	5.3
ZM	Eutectic	0.4	1.1	5.9
	Zn crystal	0.4	0.4	5.7

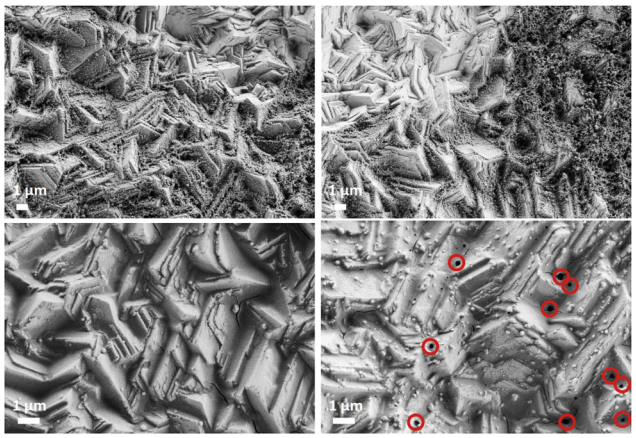

Fig. 2 SEM images of ZE coated with PT 1 (top) and PT 2 (bottom) after alkaline cleaning (left) and acidic cleaning (right). Formed pores have been highlighted by red circles.

Fig. 3 shows comparable SEM images of Z substrate coated with PT 1 or PT 2 after alkaline cleaning as well as after acidic cleaning (corresponding images for this and other substrates after cleaning but before CC are available in the associated doctoral thesis[42]). The microstructure of the substrate differs compared to the ZE substrate but the conversion layer formed on Z substrate with PT 1 is heterogeneous, too. Again, a porous network is formed with optical higher density in surface indentations, resulting from the skin-pass rolling process step of the surface. After acidic cleaning, the structure formed is finer and has an optically higher density in indentations. The application of PT 2 results, as well, in a heterogeneous surface coverage. A thin film has built up on the surface in which particles have formed. These particles were mainly observed in the indentation of the surface and there is no significant difference visible when using either an alkaline cleaner or an acidic one.

The SEM images of ZM coated with PT 1 or PT 2 after alkaline cleaning as well as acidic cleaning are shown in

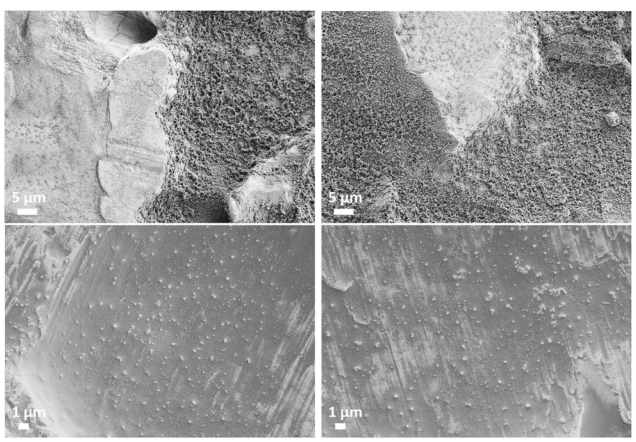

Fig. 3 SEM images of Z coated with PT 1 (top) and PT 2 (bottom) after alkaline cleaning (left) and acidic cleaning (right).

Fig. 4. SEM images of a sample before applying the corrosion protection oil (not shown) appear visually similar to those after alkaline cleaning. The conversion layer formed on ZM with PT 1 is heterogeneous just as seen on the other substrates. A porous network comparable to what was observed on the Z surface is formed whereby there is no coverage around the zinc crystals. After acidic cleaning, the formed structure is finer and has a higher density whereas after alkaline cleaning, the formed structures appear more strongly cross-linked. The differences between the two surfaces are especially obvious when looking at higher magnification (middle row in Fig. 4). PT 2 gives a heterogeneous surface coverage where a thin film has built up on the surface in which particles have formed in addition. These particles are mainly observed in the indentations of the surface and more particles are observed after the acidic cleaning.

3.2 Effect of rinsing on pretreatment layer

The layer formation behaviour was investigated taking SEM images while the coating weight was determined with GDOES measurements. These measurements confirm the hypothesis that rinsing removes pretreatment components from the surface. Both rinsing steps wash off parts of the CC, as evidenced by the values for both marker elements, phosphorous for PT 1 (Fig. 5) and titanium for PT 2 (Fig. 6). When using PT 1 all substrates show similar results after alkaline cleaning. A rinsing a. c. removes up to 35% of the coating whereas up to 10% less will be detached when rinsing follows drying compared to no rinsing. The acidic cleaning leads to higher removal with values up to 60% when rinsing a. c. After the drying process, more CC remains on the surface when using Z and ZM substrates. On ZE substrate, a similar amount of CC can be rinsed off in both rinsing steps.

The usage of PT 2 causes a much higher removal after the alkaline cleaning when rinsing a. c. where up to 75% of titanium can be rinsed off on all substrates. After the drying process, these values vary a lot on the different substrates. Most of PT 2 can be rinsed off the ZE substrate whereas only up to 10% can be dissolved from the ZM substrate. The acidic cleaning leads to higher removal rates when rinsing a. d. with variations between 45% on ZM substrate and up to 70% on ZE substrate. The amount of the respective marker

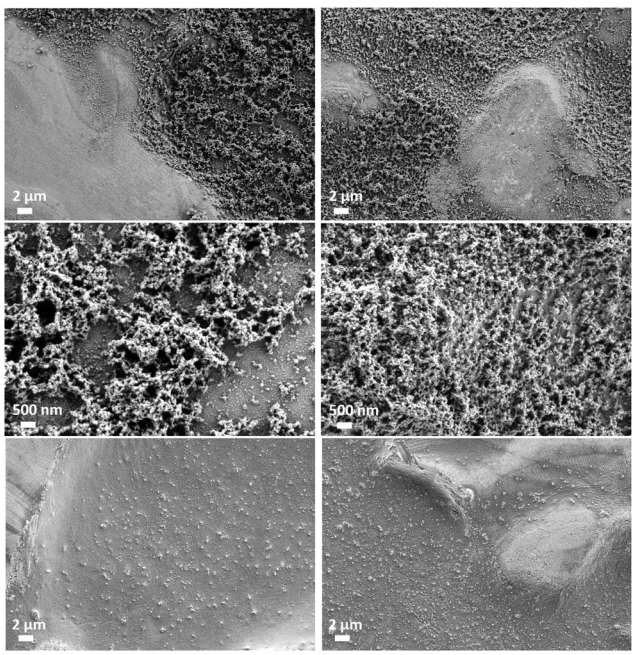

Fig. 4 SEM images of ZM coated with PT 1 (top and middle; middle with higher magnification) and PT 2 (bottom) after alkaline cleaning (left) and acidic cleaning (right).

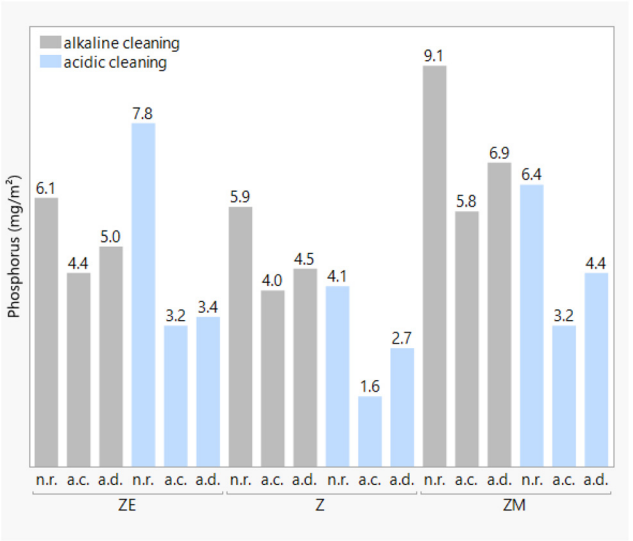

Fig. 5 GDOES results for marker element phosphorus of PT 1. Differentiation between n. r., a. c. and a. d.

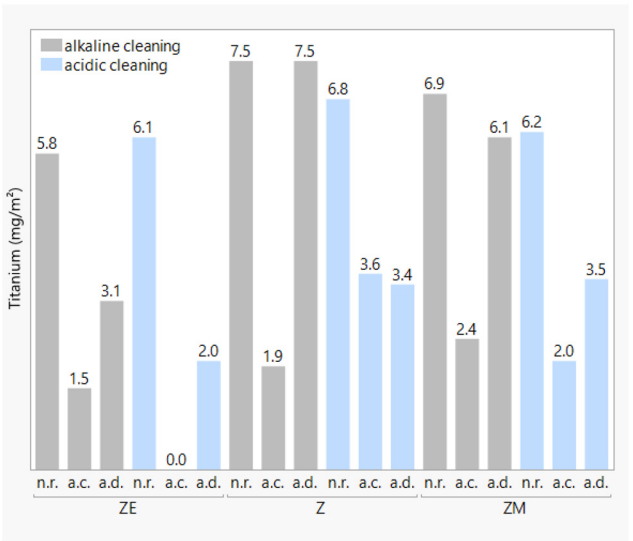

Fig. 6 GDOES results for marker element titanium of PT 2. Differentiation between n. r., a. c. and a. d.

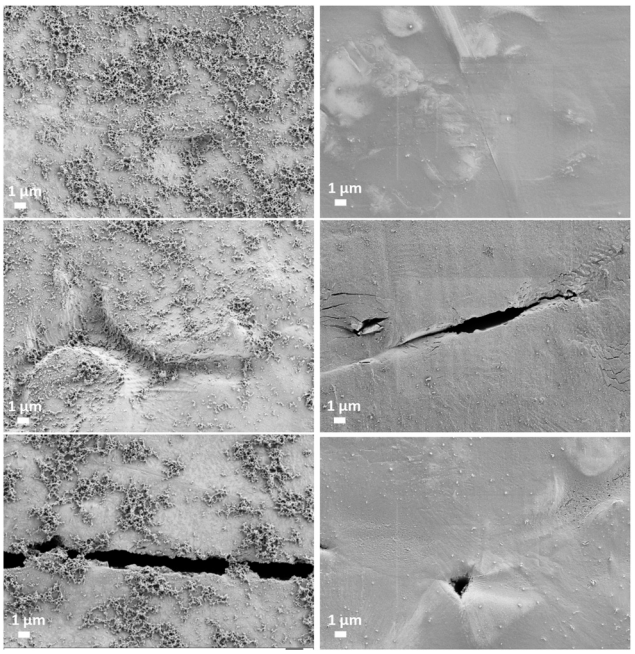

Fig. 7 SEM images of ZM coated with PT 1 (left) and PT 2 (right) without rinsing (top), with rinsing a. c. (middle) and rinsing a. d. (bottom).

element is in general higher after alkaline cleaning for Z and ZM substrate as well as for both pretreatment solutions used. Only the value on ZE after acidic cleaning without rinsing does not align with this observation. All determined values of the non-rinsed samples are in agreement with the CC marker elements target weights.

Fig. 7 shows the associated SEM images taken of the coated ZM substrate. The rinsing steps lead to fewer typical surface features like shown above and the coverage of the surface with both CCs gets reduced. The difference is more significant when rinsing directly after the roll-coater due to the fact that the water-based pretreatment solution is not fully dried at this step and therefore more susceptible to rinsing. As described above, PT 1 has a net-like structure which covers parts of the surface. The rinsing step directly after the laboratory roll coater leads to formation of an optically thinned out structure. If the sample has been dried first, the conversion layer shows its typical net-like structures with areas including higher density and cross-linking, just as without rinsing.

PT 2 shows a similar behavior where the rinsing directly after the application by laboratory roll-coater leads to fewer formation of typical surface features like shown above and the coverage of the surface seems to get less

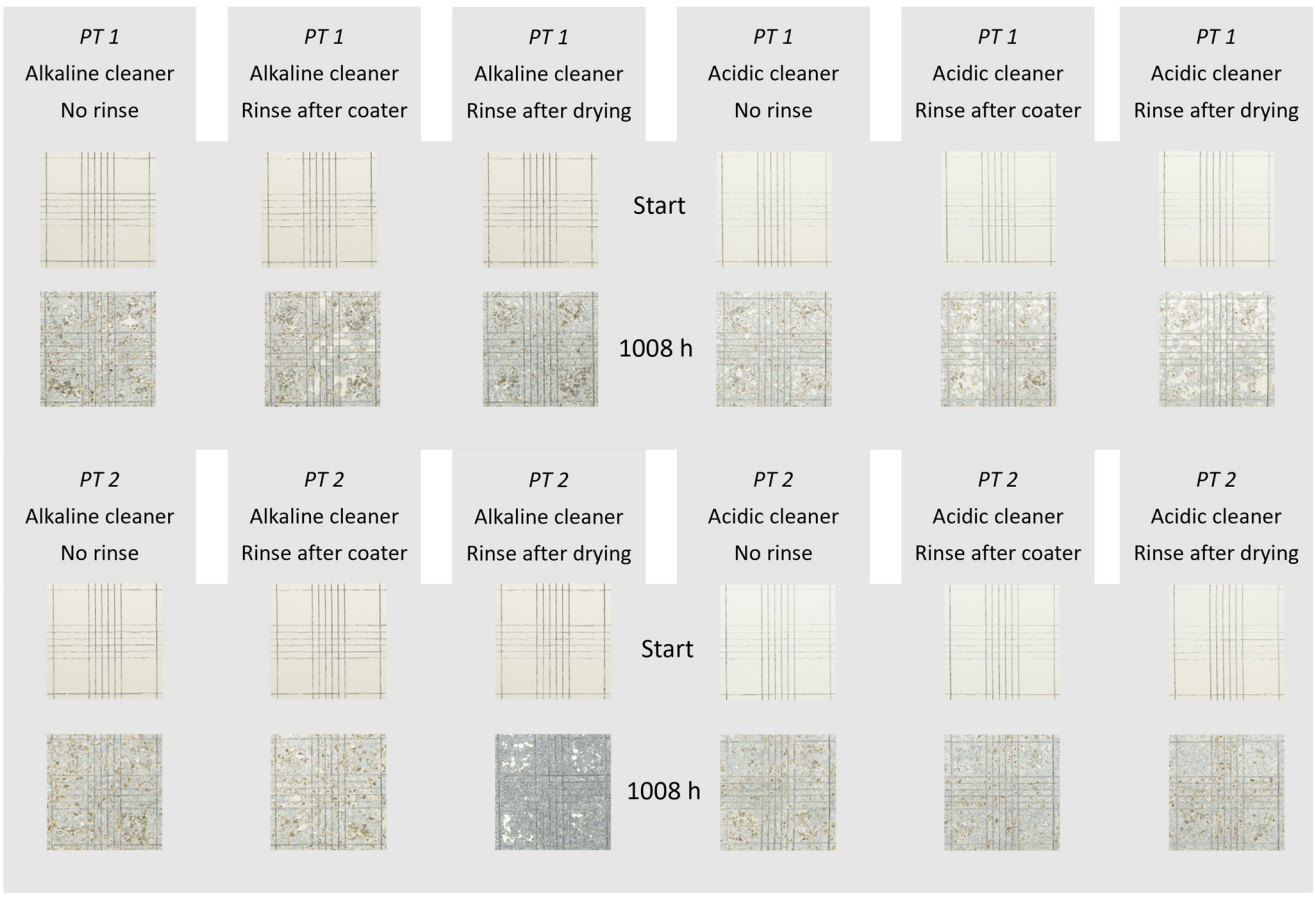

Fig. 8 Visual images of coated samples before and after water storage test for 1008 h (6 weeks) for ZM substrate.

since eutectic phases from the ZM substrate are revealed. If the sample was rinsed after drying in a continuous furnace the coverage was similar with more particles that have been grown in the layer. The SEM images taken on ZE and Z show comparable results for both pretreatment solutions.

3.3 Adhesion testing of fully coated substrates

For assessing the effect of pretreatment on coating stability, a water-storage test of fully coated substrates was performed. All test results are presented in Fig. 8–10. In this study, the paint adhesion is qualitatively assessed as the amount of coating that cannot be removed in the cross-cuts after a certain time. If no paint removal is possible, the adhesion can be described as excellent whereas it is not sufficient when the substrate gets visible. It should be pointed out here that the area of detached coatings is not quantified in this work, however, main differences are clearly visible.

Most of the coating was removed from ZM substrates (Fig. 8). Differences occur when comparing the results of samples that have been coated with PT 1 but have been cleaned differently. The acidic cleaning leads to a better paint adhesion whereby the best effect can been seen in combination with a rinsing step a. d. When using an alkaline cleaner, the rinsing a. c. gives the best paint adhesion. In comparison, PT 2 shows worse results, with insufficient adhesion; thus the usage of PT 1 improves paint adhesion. Also, there is little effect of cleaning or rinsing when using PT 2 on ZM and the coating can be removed almost completely. For ZM after alkaline cleaning, rinsing steps have no beneficial effect on the paint adhesion within the accuracy achieved by visual inspection.

Fig. 9 and 10 show the results of the water storage test when using Z and ZE substrates coated with PT 1 and PT 2. Clearly, the paint adhesion is better compared to the ZM substrate. There is little paint removal from Z substrate which has been coated with PT 1 and a higher delamination on samples that have been coated with PT 2. A marginal difference between rinsed and non-rinsed samples is visible for acidic cleaning whereby the no rinse procedure leads to a slightly better adhesion. For alkaline cleaning, differences were not so clear for PT 1 whereas there is an improved adhesion for PT 2 when rinsing is performed after drying. The best results were obtained for the ZE samples. No visual removal of the paint indicates an excellent adhesion to the substrate for both pretreatment solutions and both cleaning versions.

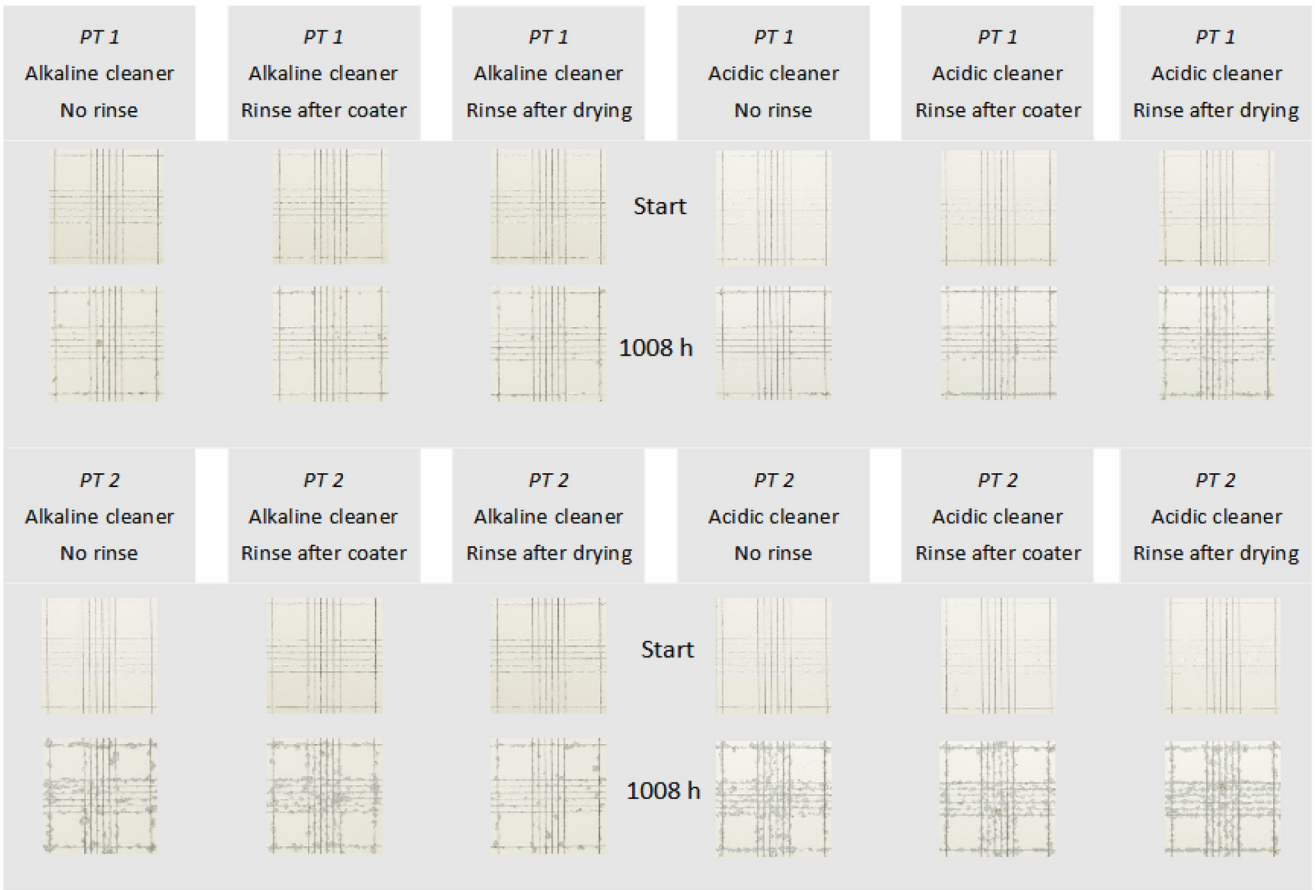

Fig. 9 Visual images of coated samples before and after water storage test for 1008 h (6 weeks) for Z substrate.

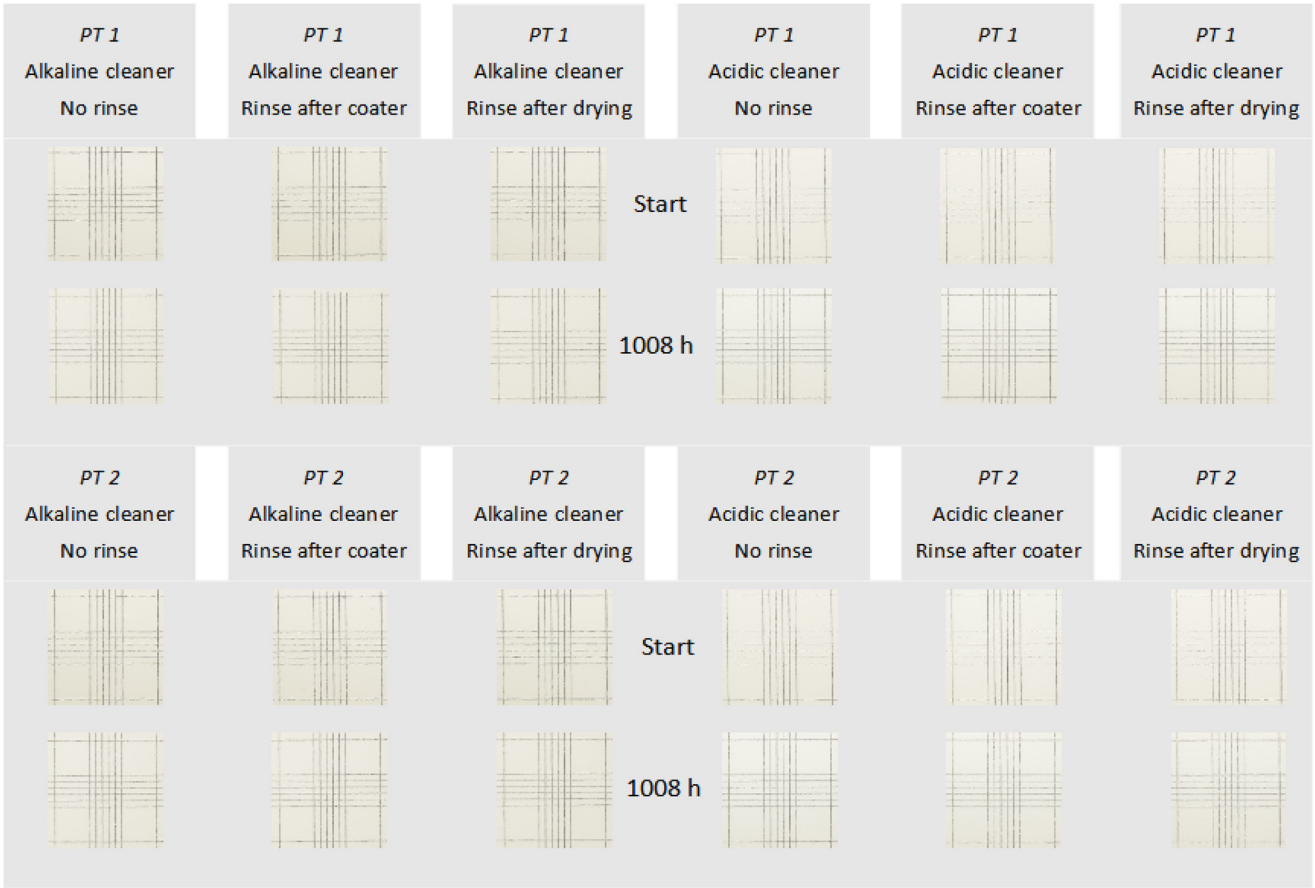

Fig. 10 Visual images of coated samples before and after water storage test for 1008 h (6 weeks) for ZE substrate.

3.4 Pretreatment layer formation on model substrates

For a better understanding of the alloy elements' role and their effect on the conversion layer build-up, model surfaces have been generated. Images of the complete surface are shown in Fig. 11. These images show clear visual differences between these surfaces. For the investigated metallic coating substrates ZE, Z and ZM, a white film had formed on their surface. On the zinc model surface, a white film spanning over most of the surface is obvious in Fig. 11 (top left). On aluminium on the other hand, the surface became dark (Fig. 11, top right). The magnesium model surface was white in the middle of the sample and brownish closer to the rim (Fig. 11, bottom). The difference on the magnesium model surface might be caused by a varying amount of CC and different film morphologies in the different areas.

SEM images taken of these model surfaces after application of PT 1 by spin-coating and drying at room temperature are shown in Fig. 12. The typical porous network structure of PT 1, which was observed on the industrial substrates is also obtained on the zinc coated surface as well as on the magnesium coated surface. At the same time, the typical PT 1 network formation is visually more dense on the zinc coated surface. On magnesium, there are different growth states of the PT 1 network when comparing areas closer and further away from the edge. These differences could be explained by the high reactivity of magnesium and the transport of fluid towards the edge of the sample during

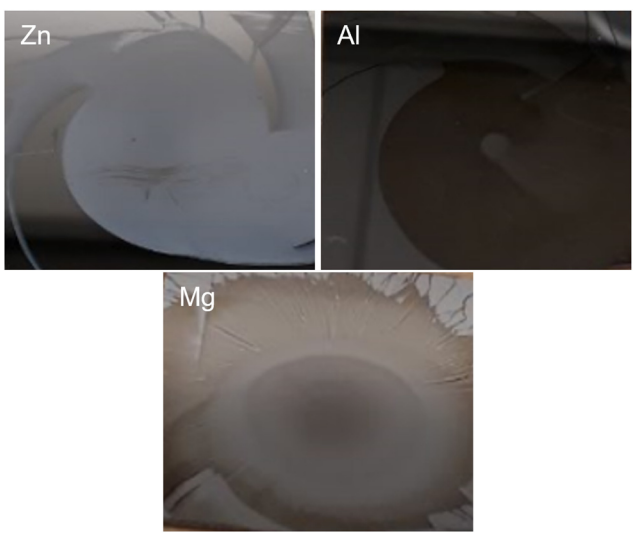

Fig. 11 Visual images of model surfaces (45 mm × 45 mm) of zinc, aluminium or magnesium, coated with PT 1 by spin-coating, after drying.

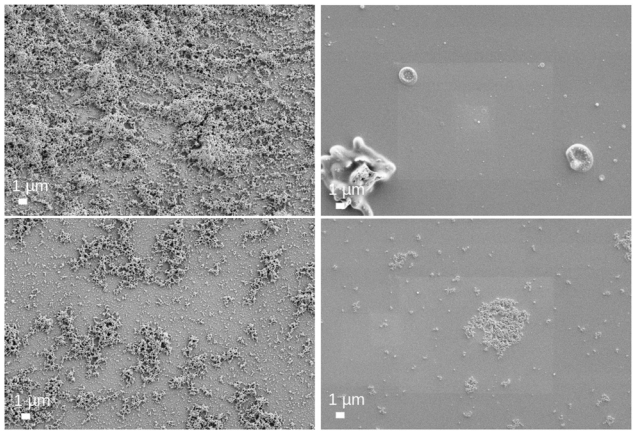

Fig. 12 SEM images of model surfaces coated with PT 1 on zinc (top left), aluminium (top right) or magnesium (bottom). Magnesium – center of the sample (bottom left) and area closer to the edges (bottom right).

the spin coating process so that reaction and transport kinetics lead to a structuring on the macroscale. No network formation was detected on the aluminium surface, just a smooth layer.

4 Discussion

4.1 Pretreatment layer formation

The SEM images shown in Fig. 2 reveal that the cleaning step has a visible effect on the nano-conversion layer's homogeneity. Especially the acidic cleaning leads to areas on the surface where no conversion layer build-up is taking place. The surface roughness determined by AFM confirmed that the ZE surface loses its roughness when aggressive cleaning solutions were used.

A smoother surface could lead to poorer wettability since the surface area is smaller. This difference could explain the areas free of CC when PT 1 was used. The differences in results for PT 2 coated surfaces might be caused by higher reaction rates, since there is a significantly higher number of particles when an acidic cleaning was performed. In addition, more pores are formed which could be explained by hydrogen evolution that is playing a crucial role in the process of layer formation of CCs.[6] A possible conclusion might be an accelerated conversion layer formation on acid cleaned ZE surfaces. After an acidic cleaning step the CC structure on PT 1 is finer and more dense (Fig. 3). The typical net-like structure can mainly be found in the surface indentations which suggests that the surface morphology has a significant impact on the CC formation. In contrast, the alkaline cleaning does not lead to a difference in conversion layer build-up when using PT 2.

On ZM surfaces there is the same effect of the surface morphology as on Z surfaces. The typical pretreatment layer formation takes place in the surface indentations and the resulting structure is finer and more dense after the acidic cleaning when using PT 1. Marginal differences can be seen in the SEM images taken of PT 2 coated surfaces where only the number of particles varies between the different cleaning solutions. Varying surfaces chemistries as well as the differences in surface morphologies might be able to explain differences in the conversion layer build-up.

When it comes to the conversion layer build-up, there are little differences between Z and ZM which can be explained by similarities in their surface morphologies. Significant amounts of CC could be rinsed off directly after the laboratory roll coater as well as after the drying in a continuous furnace. A rinsing step led to the removal of coating components that have not reacted with the substrate and continue to be present on the surface without any cross-linking. GDOES measurements (Fig. 5 and 6) confirmed that more of the CC was removed when the rinsing step was performed directly after the laboratory roll coater. On the one hand, the quite short conversion time of just a few seconds could be insufficient for extended cross-linking within the layer. Surprisingly, though, significant amounts of the coating could be removed even after the drying step.

The drying in a continuous furnace should lead to the removal of water in the CC layer and end conversion reactions. The resulting conversion layer should adhere sufficiently to the metal surface. There was no clear difference in removal of components between the differently galvanised steel substrates investigated here since it was possible to remove significant amounts of CC on all three surfaces. A possible effect of wetting kinetics and the kinetics of the dissolution of the initial oxide film and its impact on CC adhesion cannot be ruled out based on the results from this work.

In this work, the bare aluminium surface shows little traces of CC, even though similar CCs are commonly used for the pretreatment of aluminium alloys.[6] From the substrates investigated here, both Z and ZM contain aluminium in the surface,[34,37] but ZM has a much higher aluminium content compared to Z. ZE substrates do not contain any aluminium. Aluminium content in the surface oxide itself can thus not be solely responsible for the observed differences in CC and coating adhesion. A study involving secondary ion mass spectrometry (SIMS) of similar ZM substrates showed Al to be dominating after acidic cleaning in sulfuric acid whereas after alkaline cleaning in NaOH, the Al concentration decreases and Zn and Mg are strongly present on the surface of zinc grains.[39] SIMS analysis conducted in parallel to this work showed that for acid cleaned ZM surfaces, Zn is dominant on the surface, with some regions containing Al in addition.[42] After alkaline cleaning, there is presumably a difference in surface composition between eutectic phase and zinc phase, with the latter showing Zn and Mg on the surface and the former Zn and Al.[42]

Different CC structures on the different galvanised substrates observed in this work could thus be related to wetting kinetics due to the short contact time, which may need to be adjusted for various substrates, rather than

specific features of the surface composition. For CCs formed under immersed conditions on aluminium, an effect of convection on formation kinetics is well established.[43,44]

4.2 Coating adhesion as consequence of CC structure

One could argue that components not chemically bound to the metal surface could negatively impact paint adhesion. The results from fully coated metals (Fig. 8–10) reveal that the rinsing affects the corrosion protection performance. Especially on the ZM surface, a clear improvement of the paint adhesion was found when rinsing after the laboratory roll coater as well as after the drying in a continuous furnace in combination with the use of PT 1. The paint adhesion on ZM surfaces was found to be improved when using an acidic cleaning solution. On the other hand, there was no significant effect visible when using PT 2 since all samples led to insufficient paint adhesion. The corrosion performance on Z surfaces was better in comparison to ZM surfaces in all conducted experiments.

On all Z surfaces a very good paint adhesion was observed. The alkaline cleaning step leads to marginal better results. The best adhesion was obtained when the sample was rinsed directly after the laboratory roll coater. After acidic cleaning, the rinsing leads to slightly worse paint adhesion, especially the rinsing after the drying in a continuous furnace. Since the surface morphology on Z and ZM and the galvanised coating thickness are comparable, the differences in the paint adhesion might be explained by differences in their surface composition. ZE surfaces have a different surface morphology and surface composition; no paint delamination was found. This observation is independent whether it was cleaned by an alkaline cleaning step or an acidic cleaning step. In addition there was no effect regardless of which pretreatment solution was used or whether the substrate was rinsed after the CC. An additional test was done in which no CC has been used. Thus, the ZE surface was coated with a primer and a top coat directly after cleaning. In this situation, the resulting paint adhesion was excellent, too. In comparison to Z or ZM, the pure zinc coating of ZE has a higher surface area which might be one factor contributing to its excellent paint adhesion.

To be able to explain these described differences in more detail, model samples with smoother surfaces of the elements zinc, aluminium or magnesium were prepared. The resulting conversion layer built-up on zinc and magnesium surfaces was corresponding to the typical net-like formation of PT 1 that was found on the galvanised steel substrates. In contrast, there was no such conversion layer built-up on aluminium even though the samples have been coated, but with a smoother layer. This investigation leads to the hypothesis that aluminium might hinder the network formation that is necessary for good paint adhesion. Z and ZM contain aluminium.[34,37] In various experiments, CC formation of similar prototypical systems was observed on aluminium prepared by physical vapour deposition,[45] so that the aluminium content alone cannot be responsible for the observed differences. In particular, aluminium was found to be included in the conversion layer by detailed surface analysis on Z.[34] Also the oxides formed on Z differ from the oxides formed on ZM surfaces, so that the microstructure and its chemical composition on these two substrates is not the same.

One study concluded that ZrO_2 nucleation started from aluminium-rich domains on galvanised steel,[46] suggesting that some additives in the pretreatments used here may modify specifically the interaction between aluminium and the conversion layer formed during pretreatment. In general, differences in the deposition kinetics on different surfaces, comparing, *e.g.*, galvanised steel and aluminium alloys, are well established.[47]

There is no indication that the insolubility of magnesium oxide during alkaline treatment is leading to poor paint adhesion on ZM, based on the small differences in results between acidic and alkaline treatment. Under acidic conditions, magnesium oxide is soluble, however, the differences between alkaline and acidic cleaner are small. However, on zinc–aluminium–magnesium alloys, a standard commercial alkaline cleaner was found to dissolve magnesium from $MgZn_2$ intermetallic particles.[48]

There is also no direct evidence that formation of a spinel type mixed aluminium magnesium oxide on ZM leads to reduced CC formation. Spinel type oxides have been observed on magnesium-containing aluminium alloys under certain conditions; their chemical stability is positive for corrosion protection but problematic for CC formation.[49,50] They may also be present in ZM coatings.[40] However, pure evaporated aluminium shows the least signs of coating formation, whereas pure magnesium shows typical signs of reactions with the solutions.

5 Conclusion

Acidic cleaning leads to a better conversion layer build-up for one of the two investigated conversion layers PT 1 on Z and ZM substrates whereas the layer formation was more heterogeneous on ZE surfaces. The effect of cleaning when using PT 2 was less distinct at the different pH but the inclusion of a rinsing step in the coating process affects the CC wetting behavior of both pretreatment solutions used. Even after the drying of the substrates in a continuous furnace, significant amounts of the conversion layer can be removed. Accordingly, a rinsing step can improve the paint adhesion of the full coat system especially on ZM surfaces. No conversion layer is needed on ZE surfaces to achieve an excellent paint adhesion. Summarising the results on industrially produced metallic coatings, the traditional ZE is the most robust showing excellent coating adhesion independent of cleaning and pretreatment. The modern ZM shows best coating adhesion after acidic cleaning, treatment

with PT 1 and rinsing. For Z, PT 1 shows best adhesion as well, independent of cleaning type.

The utilization of model surfaces enabled to gather evidence that there is a different effect of each individual metal used here, *i.e.* zinc, magnesium or aluminium, on the CC wetting behavior. Surprisingly, it is aluminium and not magnesium that hinders the typical network formation of PT 1; the working hypothesis that the presence of magnesium yields poor adhesion was therefore not confirmed. Overall it was shown that the cleaning step of the metal surfaces has not only a significant impact on the conversion layer build-up but also on the paint adhesion in general. The surface morphology as well as the surface composition affect the conversion layer formation. To that end, a logical next step would be a quantitative investigation of the adhesion on the different phases that are part of the microstructure of the included metallic coatings and possibly a more comprehensive comparison to other aluminium-rich metallic coatings. Effects of the wetting kinetics during roll-to-roll application with subsequent drying may also be important for observed differences. With correct pretreatment choice, the novel ZM substrate can thus be protected.

Author contributions

Conceptualization, investigation and formal analysis (LMB), supervision (AE, MR), writing of the original draft (LMB), reviewing and editing (LMB, AE, MR).

Conflicts of interest

LMB is currently employed at a manufacturer of pretreatments. AE has other industry collaborations concerning pretreatments.

Data availability

The data supporting this article have been included as part of the article.

Acknowledgements

The authors would like to thank thyssenkrupp Steel Europe AG for financing. LMB thanks the working group pre- and post-treatment for providing this topic, her supervisors for helpful discussions, and the surface analytical team for GDOES investigations.

Notes and references

1 P. Maaß and P. Peißker, *Handbuch Feuerverzinken*, Wiley-VCH, Weinheim, Germany, 2008.
2 K.-P. Müller, *Lehrbuch Oberflächentechnik*, Vieweg+Teubner, Wiesbaden, Germany, 1996.
3 H.-W. Zoch and G. Spur, *Handbuch Wärmebehandeln und Beschichten*, Hanser, München, Germany, 2015.
4 B. Meuthen and A.-S. Jandel, *Coil–Coating*, Springer Vieweg, Wiesbaden, Germany, 2013.
5 C. D. Fernández-Solis, A. Vimalanandan, A. Altin, J. S. Mondragón-Ochoa, K. Kreth, P. Keil and A. Erbe, in *Soft Matter at Aqueous Interfaces*, ed. P. R. Lang and Y. Liu, Springer, Cham, Switzerland, 2016, *ch. 2 - Fundamentals of Electrochemistry, Corrosion and Corrosion Protection, Lect. Notes Phys.*, vol. 917, pp. 29–70.
6 I. Milošev and G. S. Frankel, *J. Electrochem. Soc.*, 2018, **165**, C127–C144.
7 G. Yoganandan, K. Pradeep Premkumar and J. Balaraju, *Surf. Coat. Technol.*, 2015, **270**, 249–258.
8 N. Khun and G. Frankel, *Mater. Corros.*, 2015, **66**, 1215–1222.
9 H. Ardelean, I. Frateur and P. Marcus, *Corros. Sci.*, 2008, **50**, 1907–1918.
10 A. Ghanbari and M. Attar, *J. Coat. Technol. Res.*, 2015, 1–11.
11 S. Sharifi Golru, M. Attar and B. Ramezanzadeh, *Appl. Surf. Sci.*, 2015, **345**, 360–368.
12 H. Asemani, P. Ahmadi, A. Sarabi and H. Eivaz Mohammadloo, *Prog. Org. Coat.*, 2016, **94**, 18–27.
13 A. Ghanbari and M. Attar, *Surf. Coat. Technol.*, 2014, **246**, 26–33.
14 P. Taheri, K. Lill, J. de Wit, J. Mol and H. Terryn, *J. Phys. Chem. C*, 2012, **116**, 8426–8436.
15 H. Eivaz Mohammadloo, A. Sarabi, R. Mohammad Hosseini, M. Sarayloo, H. Sameie and R. Salimi, *Prog. Org. Coat.*, 2014, **77**, 322–330.
16 A. Sarfraz, R. Posner, M. M. Lange, K. Lill and A. Erbe, *J. Electrochem. Soc.*, 2014, **161**, C509–C516.
17 A. Sarfraz, R. Posner, A. Bashir, A. Topalov, K. J. J. Mayrhofer, K. Lill and A. Erbe, *ChemElectroChem*, 2016, **3**, 1415–1421.
18 Z. Gao, D. Zhang, Z. Liu, X. Li, S. Jiang and Q. Zhang, *J. Coat. Technol. Res.*, 2019, **16**, 1–13.
19 L. Fockaert, M. Ankora, J. Van Dam, S. Pletincx, A. Yilmaz, B. Boelen, T. Hauffman, Y. Garcia-Gonzalez, H. Terryn and J. Mol, *Prog. Org. Coat.*, 2020, **146**, 105738.
20 E. Mysliu, K. Sletteberg Storli, H. M. Skogøy, S. Kubowicz, I.-H. Svenum, O. Lunder and A. Erbe, *Electrochim. Acta*, 2024, **477**, 143805.
21 V. Saarimaa, A. Markkula, K. Arstila, J. Manni and J. Juhanoja, *Adv. Mater. Phys. Chem.*, 2017, **7**, 28–41.
22 S. Adhikari, K. A. Unocic, Y. Zhai, G. Frankel, J. Zimmerman and W. Fristad, *Electrochim. Acta*, 2011, **56**, 1912–1924.
23 J. Gray and B. Luan, *J. Alloys Compd.*, 2002, **336**, 88–113.
24 M. Nabizadeh, K. Marcoen, E. A. M. Cherigui, M. D. Havigh, T. Kolberg, D. Schatz, H. Terryn and T. Hauffman, *Appl. Surf. Sci.*, 2023, **610**, 155554.
25 A. Abrashov, V. Sukhorukova, N. Grigoryan, A. Sundukova, O. Grafov and T. A. Vagramyan, *Int. J. Corros. Scale Inhib.*, 2023, **12**, 1374–1391.
26 P. D. Deck and D. Reichgott, *Metal Finish*, 1992, **90**, 29–35.
27 H. Hubert, H. Puderbach, H. Pulm and W. Roland, *Fresenius' Z. Anal. Chem.*, 1989, **333**, 304–307.
28 M. Sababi, H. Terryn and J. Mol, *Prog. Org. Coat.*, 2017, **105**, 29–36.

29 L. Fockaert, S. Pletincx, D. Ganzinga-Jurg, B. Boelen, T. Hauffman, H. Terryn and J. Mol, *Appl. Surf. Sci.*, 2020, **508**, 144771.
30 S. Le Manchet, D. Verchère and J. Landoulsi, *Thin Solid Films*, 2012, **520**, 2009–2016.
31 X. Liu, D. Vonk, H. Jiang, K. Kisslinger, X. Tong, M. Ge, E. Nazaretski, B. Ravel, K. Foster, S. Petrash and Y.-C. K. Chen-Wiegart, *ACS Appl. Nano Mater.*, 2019, **2**, 1920–1929.
32 X. Liu, D. Vonk, K. Kisslinger, X. Tong, G. Halada, S. Petrash, K. Foster and Y.-C. K. Chen-Wiegart, *ACS Appl. Mater. Interfaces*, 2021, **13**, 5518–5528.
33 M. Nabizadeh, K. Marcoen, E. A. Mernissi Cherigui, T. Kolberg, D. Schatz, H. Terryn and T. Hauffman, *Surf. Coat. Technol.*, 2022, **441**, 128567.
34 V. Cristaudo, K. Baert, P. Laha, M. Lyn Lim, E. Brown-Tseng, H. Terryn and T. Hauffman, *Appl. Surf. Sci.*, 2021, **562**, 150166.
35 L. Li, A. L. Desouza and G. M. Swain, *Analyst*, 2013, **138**, 4398–4402.
36 L. Li, B. W. Whitman and G. M. Swain, *J. Electrochem. Soc.*, 2015, **162**, C279–C284.
37 N. Le Bozec, D. Thierry, M. Rohwerder, D. Persson, G. Luckeneder and L. Luxem, *Corros. Sci.*, 2013, **74**, 379–386.
38 G. A. C. Sartori, B. Remy, T. M. Amorim and P. Volovitch, *Metals*, 2025, **15**, 476.
39 B. W. Çetinkaya, F. Junge, G. Müller, F. Haakmann, K. Schierbaum and M. Giza, *J. Mater. Res. Technol.*, 2020, **9**, 16445–16458.
40 M. Arndt, J. Duchoslav, H. Itani, G. Hesser, C. Riener, G. Angeli, K. Preis, D. Stifter and K. Hingerl, *Anal. Bioanal. Chem.*, 2012, **403**, 651–661.
41 H. Kijima and N. Bay, *Int. J. Mach. Tools Manuf.*, 2008, **48**, 1313–1317.
42 L.-M. Baumgartner, *PhD thesis*, Ruhr-Universität Bochum, Bochum, Germany, 2022, DOI: **10.13154/294-9958**.
43 O. Lunder, C. Simensen, Y. Yu and K. Nisançioğlu, *Surf. Coat. Technol.*, 2004, **184**, 278–290.
44 J. Cerezo, R. Posner, I. Vandendael, J. de Wit, H. Terryn and J. Mol, *Mater. Corros.*, 2016, **67**, 361–367.
45 F. George, P. Skeldon and G. Thompson, *Corros. Sci.*, 2012, **65**, 231–237.
46 C. S. Velasquez, E. P. S. Pimenta and V. F. C. Lins, *J. Mater. Eng. Perform.*, 2018, **27**, 2138–2147.
47 J. Cerezo, I. Vandendael, R. Posner, K. Lill, J. De Wit, J. Mol and H. Terryn, *Surf. Coat. Technol.*, 2013, **236**, 284–289.
48 J. Han, D. Thierry and K. Ogle, *Surf. Coat. Technol.*, 2020, **402**, 126236.
49 Z. Jia, B. Graver, J. C. Walmsley, Y. Yu, J. K. Solberg and K. Nisancioglu, *J. Electrochem. Soc.*, 2008, **155**, C1–C7.
50 S. Kumari, S. Wenner, J. C. Walmsley, O. Lunder and K. Nisancioglu, *J. Electrochem. Soc.*, 2019, **166**, C3114–C3123.